RSC Advances

PAPER

View Article Online
View Journal | View Issue

Cite this: *RSC Adv.*, 2020, **10**, 9070

Novel non-mulberry silk fibroin nanoparticles with enhanced activity as potential candidate in nanocarrier mediated delivery system†

Rashmi Rekha Baruah,[a] Mohan Chandra Kalita[b] and Dipali Devi *[a]

Received 29th October 2019
Accepted 21st January 2020

DOI: 10.1039/c9ra08901b

rsc.li/rsc-advances

Silk fibroin (SF) is well known for its excellent biocompatible properties facilitating its application in the field of biomedical engineering through different biomaterial fabrications in the recent era. Here in this study, novel nanoparticles from non-mulberry SF of *Antheraea assamensis* were fabricated, characterized and evaluated for its applicability as nanocarrier. Fabricated nanoparticles were initially compared with prevailing SF nanoparticles from *Bombyx mori*. Fabricated *A. assamensis* silk fibroin nanoparticles (AA-SFNps) were found to be lesser in size (80–300 nm in diameter) than *B. mori* silk fibroin nanoparticles (BM-SFNps) (120–500 nm in diameter). When checked for stability, AA-SFNps were found to be more stable than BM-SFNps in biological media. FTIR and XRD studies revealed persistence of structural properties even after fabrication. TGA and DSC studies showed AA-SFNps to be thermally more stable than BM-SFNps without any cytotoxicity (MTT assay). On loading with model drug Doxorubicin hydrochloride (DOX), AA-SFNps exhibited an encapsulation efficiency of 94.47% with 11.81% loading of the anticancer drug. Cumulative release study revealed highest percentage release of DOX (42.1 ± 0.4%) at pH 5.2 on day 7 in comparison to pH 7.4 and 8.0. Sustained release profile of the DOX loaded AA-SFNps (AA-SFNps-DOX) was clearly reflected and it was found to be highly cytotoxic against triple negative MDA-MB-231 cells in comparison to free DOX at different time points. Overall, this study showed the efficacy of the AA-SFNps as a nanocarrier for future drug delivery applications.

Introduction

Nanocarriers play a vital role as an effective delivery system for a therapeutic drug by enhancing the efficiency of the drug through controlled delivery thereby reducing the problems associated with dose-dependent toxicity and encouraging the sustained release of the drug to the target site.[1–4] Silk proteins provide an efficient platform in this field due to their non-cytotoxic, biocompatible, biodegradable and non-immunogenic properties.[5–8] Silk nanocarriers have been used as a biomedicine in combination with a specific drug.[9,10] Mulberry SF from *B. mori* was widely explored in this regard. Nanoparticles which were fabricated using mulberry SF from *B. mori* and loaded with different drugs like platinum(IV) prodrug, 5-fluorouracil, curcumin, paclitaxel, methotrexate, floxuridine and doxorubicin *etc.* for successful carrier-based delivery systems were extensively reported (Table 1).[2,3,11–17]

The non-mulberry silk fibroin nanoparticles (SFNps) from *Antheraea mylitta* and *Antheraea pernyi* have been explored as nanocarriers for effective delivery system.[18–22] Non-mulberry SF is advantageous over mulberry SF because of the presence of inherent tripeptide sequence Arg-Gly-Asp (RGD) that favours better cell attachment and proliferation through intrinsic binding protein.[23] Presence of this motif in the SF of such species makes it a good candidate for biomedical applications. *A. mylitta* SFNps loaded with folate and vascular endothelial growth factor (VEGF) have shown its potency for anticancer activity and in growth factor delivery system.[18,19] *A. pernyi* SFNps loaded with insulin and ibuprofen exhibited their effectiveness as promising materials in sustain release of the loaded drugs.[20–22]

Non-mulberry SF from *A. assamensis* have been showing potential biological activity for tissue regeneration.[24,25] *A. assamensis* silk fibroin (AA-SF) is reported to exhibit enhanced thermal and mechanical stability in comparison to all other available species of SF, which encourages the use of such proteins for future biomedical applications.[26,27] Moreover, AA-SF microparticles which were fabricated by using wet-milling and spray drying technique have been reported to be showing better cell viability with a sustained drug release profile.[28]

In the present study, non-mulberry AA-SFNps were fabricated and explored for its possible applicability to be used as

[a]*Seri-biotechnology Laboratory, Life Sciences Division, Institute of Advanced Study in Science and Technology (IASST), Paschim Boragaon, Guwahati 781035, India. E-mail: dipali.devi@gmail.com*

[b]*Department of Biotechnology, Gauhati University, Guwahati 781014, India*

† Electronic supplementary information (ESI) available: DLS and FTIR study confirming drug loading. See DOI: 10.1039/c9ra08901b

Table 1 Silk fibroin based nanocarriers for drug delivery systems

Category of silk fibroin	Species name	Drug used/studied using	Targeted against/cell line used during the study	Reference
Mulberry	*B. mori*	5-Fluorouracil, curcumin	Murine breast cancer cells (4T1)	2
		Doxorubicin	Human cervical carcinoma cells (HeLa)	11
		Curcumin	Breast cancer cell lines MCF-7 (Her2−), MDA-MB-453 (Her2+)	12
		Doxorubicin	Human breast adenocarcinoma cell line (MCF-7), multidrug resistant (MCF-7/ADR)	3
		Paclitaxel	Human gastric cancer cell lines BGC-823 and SGC-7901	13
		Floxuridine	Human cervical carcinoma cells (HeLa)	4
		Methotrexate	Human breast cancer cell line (MDA-MB-231)	14
		Doxorubicin	Human breast cancer cell line (MCF-7)	15
		Platinum(IV)	Human breast adenocarcinoma cell line (MCF-7, MDA-MB-231)	16
			Human breast cancer cell line (SK-BR-3)	
		Doxorubicin	Human cervical carcinoma cells (HeLa)	17
Non-mulberry	*A. mylitta*	Doxorubicin	Human breast adenocarcinoma cell line (MDA-MB-231)	18
		Vascular endothelial growth factor	Murine squamous carcinoma cell line (SCC7)	19
	A. pernyi	Doxorubicin hydrochloride	Human hepatocarcinoma cells (HepG2)	20
		Doxorubicin hydrochloride, ibuprofen and ibuprofen-Na	Murine fibroblast cell line (L-929)	21
		Insulin	No cell line used	22
	A. assamensis	Doxorubicin	Human breast adenocarcinoma cell line (MDA-MB-231)	Present study

a candidate for future drug delivery applications using DOX as a model drug. DOX is one of the most effective anthracycline drugs used for the treatment of different types of cancers.[29] In spite of its potentials, the drug has limited clinical applications because of its serious side effects arising due to dose-dependent toxicity.[30] Fabricated nanoparticles were initially characterized with dynamic light scattering (DLS), transmission electron microscopy (TEM), fourier transform infrared spectroscopy (FTIR) and X-ray diffraction (XRD) studies. Thermal properties were evaluated using thermo gravimetric analysis (TGA) and differential scanning calorimetric (DSC) assay followed by stability measurements using biological media. Initial characterization has been compared with BM-SFNps fabricated under similar conditions in order to arrive at a completely non-toxic, structurally and morphologically sound candidate. Thereafter, the nanoparticles were tested for their drug loading, release and cytotoxicity study in a dose-dependent manner. This study would provide an overall idea about the possible application of AA-SFNps for tissue engineering and as a nanocarrier for future drug delivery applications.

Experimental section

Materials and methods

Matured fifth instar larvae from non-mulberry silkworm *A. assamensis* and cocoons of mulberry silkworm *B. mori* were collected from sericulture farm of Mongoldoi District, Assam, India. Acetone was used as a desolvating agent and purchased from Merck, lithium bromide (LiBr) was purchased from HIMEDIA. Cut piece of dialysis tubing cellulose membrane (MWCO 12 kDa) and cell culture grade chemical MTT were purchased from Sigma. DMEM, fetal bovine serum (FBS), Trypsin–EDTA and Penicillin–Streptomycin antibiotics (10 000 IU ml^{-1}) were purchased from Gibco (Invitrogen, USA). DOX was purchased from Sigma Aldrich. All other tissue culture plates and flasks were purchased from Tarsons (India) for the present study.

Extraction of SF

SF was extracted from the matured 5^{th} instar larvae of non-mulberry silkworm *A. assamensis* using previously reported method.[31] Briefly, silk glands from the matured larvae were dissected out and washed with Milli-Q water. The glands were then squeezed slowly to extract the core hydrophobic fibroin followed by gentle washing in order to remove the traces of hydrophilic sericin. The extracted fibroin protein was purified by dissolving in aqueous solutions of 1% (w/v) sodium dodecyl sulfate (SDS) which was further dialyzed extensively against Milli-Q water using dialysis membrane with molecular weight cut-off (MWCO) 12 kDa in order to remove SDS from the solution. The concentration of the fibroin solution was determined by gravimetric analysis. A final concentration of 2% (w/v) solution was used for further analysis.

Mulberry *B. mori* SF solution was prepared by following earlier reported method with slight modifications.[32,33] In short, the cut pieces of cocoons were degummed in 0.02 M Na_2CO_3 solution by boiling for 1 h and washed 2–3 times with distilled water to remove the Na_2CO_3 molecules and sericin from the fibre. Degummed fibres were then dried overnight at 37 °C and further purification was carried out by dissolving the fibre at 60 °C in 9.3 M LiBr solution for 1 h. The dissolved SF solution was dialyzed against Milli-Q water with dialysis membrane MWCO 12 kDa for 3 days with regular change of water at different intervals. A final concentration of (2% w/v) was used

for further analysis of the study with concentration determined as similar as above.

Fabrication of SFNps

SFNps from *A. assamensis* and *B. mori* were prepared at room temperature using desolvation process.[34–36] In brief, an easy and single step desolvation was used to fabricate the nanoparticles by adding 10 ml of the regenerated SF (2% w/v) solution dropwise (25 μl per drop) to 10 ml acetone solution thereby making a final proportion of 1 : 1 in continuous stirring mode for 15–20 minutes. Addition of acetone results in decreasing solubility of the protein leading to precipitation in the form of nanoparticles.[37] These precipitates were harvested by 3–4 times centrifugation at 12 000 rpm for 15 min at 4 °C to remove acetone completely from the SFNps solution. The purified SFNps were re-suspended in Milli-Q water and sonicated for 15 minutes in order to get an evenly dispersed solution. The homogenised SFNps solution was then kept at −20 °C overnight and lyophilized for 8 hours. The final SFNps powder thus obtained were kept at room temperature and used for further analysis.

Characterization of SFNps

Average particle size and surface zeta potential of the SFNps were determined using dynamic light scattering (DLS) Zetasizer Nano ZS, 90 (Malvern, UK) instrument. In brief, a solution of 0.1 mg ml^{-1} of SFNps was prepared in Milli-Q water and sonicated for 30 min at 30% amplitude with a pulse rate of 5 min ON and OFF resulting in an equi-dispersed solution. This uniformly dispersed solution was used for particle size and surface zeta potential determination. Samples were repeated in triplicates ($n = 3$) and average particle size was measured as the mean diameter of the SFNps.

Morphological pattern of the AA-SFNps was studied by using TEM. 20 μl of SFNps solution (0.1 mg ml^{-1}) was used on carbon-coated electron microscopy grids. The samples were air dried in dust free environment and observed under JEOL JEM-2100 TEM with an acceleration voltage of 200 kV.

Stability of the AA-SFNps in distilled water and incomplete DMEM media was measured by determining the particle size and surface zeta potential of the nanoparticles. For this, 0.1 μg ml^{-1} of the AA-SFNps was dissolved uniformly in the solvents and incubated at 37 °C. The change in the particle size was monitored using DLS Zetasizer in two different time points (day 1 and day 10 respectively) and the data were compared with BM-SFNps under similar conditions. Experiments were repeated in triplicates ($n = 3$) for the accuracy of the results.

Evaluation of structural and thermal properties

Structural characterization of the nanoparticles was done using FTIR and XRD. For FTIR, particles were analysed using Frontier™ IR/NIR FTIR (Perkin Elmer) spectrophotometer within the spectral region from 500–4000 cm^{-1} with a resolution of 4 cm^{-1} and 32 scans per spectra. Persistence of the structural properties *i.e.* presence of amide I, amide II and amide III bonds was checked which is crucial for retaining the biological properties of the SFNps. Amorphous and crystalline nature of the SFNps were measured by using XRD. X-ray diffraction facility (PANalytical, X'PertPRO PW3040/60) instrument was used with CuKα radiation ($\lambda = 1.54$ Å) having a 2θ range within angles 5–40° with a voltage of 40 kV and 40 mA current.

Thermal stability of the AA-SFNps was determined by using Perkin Elmer, DSC 6000 (USA) instrument under a dry nitrogen gas flow of 50 ml min^{-1}. The samples were heated at 5 °C min^{-1} from 30 to 400 °C. The percentage weight loss of the SFNps was determined by TGA, using a TGA 4000 (Perkin Elmer, USA) system. Samples were heated from 30 to 800 °C with a gradual increase of 2 °C min^{-1} under inert nitrogen atmosphere. In all the above cases, a comparative study was done with BM-SFNps under similar conditions.

Biocompatibility of the SFNps

In vitro biocompatibilities of the AA-SFNps were checked using MTT (3-(4,5-dimethylthiazol-2-yl)-2,5-diphenyl tetrazolium bromide) assay. L-929 (mouse fibroblast) cells purchased from the National Centre for Cell Sciences (NCCS), Pune, India, were cultured in DMEM media, supplemented with 10% FBS, 1% IU ml^{-1} streptomycin–penicillin antibiotic solution and incubated at 37 °C in a humidified atmosphere containing 5% CO_2. Cells were used in order to obtain the optimum cell proliferation rate and morphology for the study. $\sim 1 \times 10^4$ cells were seeded in each well of 96 well plates and were incubated for 24 h under humidified atmosphere as stated above. After incubation, cells were replaced with fresh media containing SFNps of varying concentrations *i.e.* 100, 200 and 300 μg ml^{-1} and kept for another 24 h. Biocompatibility of the SFNps was determined by adding 200 μl of MTT solution (5 mg ml^{-1} of PBS at pH 7.4) and incubated for 4 h. After 4 h, solutions were removed and 200 μl of dimethyl sulfoxide (DMSO) was added to each well to solubilise the formazan crystals. The absorbance was taken at 540 nm using Thermo Scientific, Varioskan Flash 1510 spectrophotometer. The relative percentage viability of the cells was calculated considering TCP as 100%. The data were compared with BM-SFNps and after getting satisfactory results AA-SFNps were further evaluated for drug loading, release and cytotoxicity studies.

Fabrication of DOX-loaded SFNps

5 mg of AA-SFNps (equi-dispersed) in 10 ml distilled water was mixed with 0.625 mg of DOX (dissolved in 10 ml of water) to make a final volume 20 ml solution. The mixture was left in dark for an adsorption period of 20 h at room temperature under continuous stirring mode. The particle solution was then dialysed against water for about 8 hours using MWCO 12 kDa dialysis membrane to release any unbound drug. The drug-loaded nanoparticles were then centrifuged at 12 000 rpm for 10 min. The solution was washed three times to remove any unbound particles. The purified DOX-loaded nanoparticles were then lyophilised and the powder obtained was used for further study. Drug loading was confirmed using FTIR and DLS study (ESI†). For better drug loading and encapsulation efficiency, AA-SFNps : DOX proportions were optimized initially with different concentrations. Drug quantification was done

using a standard calibration curve for DOX. Drug loading and encapsulation efficiency was calculated using the formula

$$\text{Drug loading}(\%) = \frac{\text{weight of DOX in SFNps}}{\text{weight of SFNps}} \times 100\% \quad (1)$$

$$\text{Encapsulation efficiency}(\%) = \frac{\text{weight of DOX in SFNps}}{\text{weight of total DOX taken}} \times 100\% \quad (2)$$

Release study

Release study of DOX-loaded in AA-SFNps was performed at three pH concentrations (pH 5.2, 7.4 and 8). For each pH values, 1 mg of DOX-loaded nanoparticles was dispersed in 1 ml of PBS and the suspension was placed in a dialysis tube (MWCO 12 kDa) and immersed into 2 ml PBS at 37 °C in a constant shaker for 7 days. Measurements were taken at predetermined time intervals (6 h, 12 h, day 1, day 3, day 5 and day 7 respectively) and amount of DOX released was calculated by taking UV absorption measurements at 480 nm wavelength using Thermo Scientific Varioskan Flash 1510 instrument. Each time an equal volume of PBS was added back into the system to maintain the experimental conditions unchanged. All measurements were performed in triplicates and the percentage release (R) was calculated using the formula

$$R(\text{w/w})\% = \frac{\text{amount of drug released into the medium}}{\text{amount of drug loaded into particles}} \times 100\% \quad (3)$$

Cytotoxicity study of DOX-loaded nanoparticles

In vitro cytotoxicity study of free DOX and DOX-loaded nanoparticles (AA-SFNps) at various concentrations was studied using MTT assay. Human breast adenocarcinoma cells (MDA-MB-231) were purchased from the NCCS, Pune, India and grown on DMEM media, in a standard humidified atmosphere as stated above. Around 5×10^3 cells were seeded in the required wells of three different 96 well plates and kept overnight. After 24 h, media was changed with incomplete DMEM and following a 2 h interval, drug was added and each plate was kept for three different time intervals *i.e.* 24 h, 48 h and 72 h respectively under the same conditions. After specified time intervals, 200 μl of 5 mg ml^{-1} (in PBS, pH 7.4) of MTT was added to each well and incubated for 4 hours. After incubation, the plate was centrifuged at 3000 rpm for 10 min and the media was discarded and 100 μl of 100% DMSO was added into each well. The plate was incubated in a shaker for 30 min followed by absorbance taken at 540 nm using Thermo Scientific Varioskan Flash 1510 spectrophotometer. The relative percentage viability of the cells was calculated as follows considering TCP (Tissue Culture Plate, cells grown without sample) as 100%.

$$\text{Relative percentage}(\%)\ \text{viability} = \frac{[A]\text{s}}{[A]\text{c}} \times 100\% \quad (4)$$

where $[A]$s is the absorbance of the corresponding sample and $[A]$c is the absorbance of the control without sample. IC_{50} values of both free DOX and AA-SFNps-DOX at each time point was calculated from the graph equation generated after plotting the percentage inhibition against each concentration of the free drug and drug loaded nano-particles respectively ($n = 4$). The percentage inhibition was calculated using the formula

$$\text{Percentage inhibition}(\%) = \frac{[A]\text{c} - [A]\text{s}}{[A]\text{c}} \times 100\% \quad (5)$$

where, $[A]$c is the absorbance of the control without sample and $[A]$s is the absorbance of the corresponding sample.

Cell morphology study of DOX-loaded nanoparticles

Morphology of the cells at each time point was observed using LEICA DMI3000 B inverted microscope. MDA-MB-231 cells were seeded at a very low concentration *i.e.* 3000 cells per well in three different 24 well plates in DMEM media, supplemented with 10% FBS, 1% IU per ml Streptomycin–Penicillin antibiotic solution incubated at 37 °C in a humidified atmosphere containing 5% CO_2. After 24 h, media was replaced with incomplete DMEM. After 2 h interval, a drug concentration of 1 μg ml^{-1} of free DOX and AA-SFNps-DOX was added to each corresponding well of the plates and kept for three different time intervals *i.e.* 24 h, 48 h and 72 h respectively under the same conditions. In order to observe the relative effect of free drug and AA-SFNPs-DOX on MDA-MB-231 cell morphology, at each time point imaging was done using phase contrast mode ($n = 5$) and the comparative effect was evaluated.

Statistical analysis

All data were expressed as mean ± SD or mean ± standard error of mean (SEM) for $n = 3$ samples unless specified. Results were analyzed using one way ANOVA and students T-test, $^*p \leq 0.05$ was considered to be statistically significant whereas $^{**}p \leq 0.01$ and $^{***}p \leq 0.001$ was considered as highly significant. Data were interpreted using statistical software OriginPro 8 (Originlab Corporation, USA).

Results and discussion

In the present study, non-mulberry SFNps from *A. assamensis* were fabricated for the first time using single step acetone desolvation procedure (Fig. 1).[1] The fabricated SFNps were obtained with a percentage yield of 85 ± 5%. The addition desolvating agent like acetone reduces the solubility of the protein. This reduction occurs because of conformational change resulting in precipitation of silk protein. Fibroin nanoparticles from *A. assamensis* were initially compared with BM-SFNps. All the samples from both the species were collected randomly for fibroin extraction. Liquid silk fibroin extracted from non-mulberry silkworm species have shown potential biological activities.[26] BM-SFNps are well reported for its potentiality as nanocarrier under different delivery systems.[2–4,11–17] Both types of nanoparticles were evaluated for its particle size, morphology, stability, persistence of structural properties, thermal stability

and cytocompatibility in order to compare the potentiality of AA-SFNps to be used as biomaterial for future tissue engineering applications. Further, this novel nanoparticle was studied for nanocarrier mediated drug delivery systems. For this, AA-SFNPs were loaded with model drug DOX and analyzed for subsequent drug release, cytotoxicity profile and effect on morphology of human breast adenocarcinoma cells (MDA-MB-231).

Size, surface zeta potential, morphology and stability of the SFNps

The size of the SFNps was analyzed using DLS. The fabricated AA-SFNps had shown an average size range of around 185.5 ± 4.5 nm in diameter with a polydispersity index (PDI) of 0.249 ± 0.04 when measured in deionized water with 0.1 mg ml^{-1} concentration (Table 2).[16] The average size range displayed by BM-SFNps was found to be around 256 ± 7.2 nm in diameter which is slightly larger than AA-SFNps with a PDI of 0.467 ± 0.06 as determined by the light scattering particle analyzer. The average surface zeta potential of the AA-SFNps and BM-SFNps was exhibited as −27.1 ± 0.69 mV and −18.5 ± 2.5 mV respectively. Lower the surface zeta potential, more stable is the particle in colloidal solution.[11] The negative surface charge helps in increasing the rate of internalization thereby interacting with the positively charged cell surface. This encourages carrier based delivery systems for delivery of the drug into the target site.[38] The size distribution intensity as revealed by DLS and TEM showed a similar trend for both the nanoparticles (Fig. 2A and B). The result supports the size range displayed by other non-mulberry species like *A. mylitta* and *A. pernyi* in earlier reports thereby it justifies the comparable properties of the protein particles and hence strengthen its possibility to be used in drug delivery system.[20–22]

The morphology of the fabricated SFNps was assessed using TEM. Results showed a nearly spherical morphology for both AA-SFNps and BM-SFNps (Fig. 2B). The surface of the fabricated AA-SFNps exhibited a clear smooth morphological pattern in comparison to the BM-SFNps with a rough surface as displayed under TEM. The size of the nanoparticles revealed a variable range from (80–300) nm for AA-SFNps whereas BM-SFNps showed a wide size range between (120–500) nm in diameter. Mono-dispersed distributions of the particles were observed for

Table 2 Average particle size, surface zeta potential and polydispersity index of *A. assamensis* and *B. mori* SFNps ($n = 3$)

Sample name	Particle size (nm)	Zeta potential (mV)	Polydispersity index (PDI)
A. assamensis	185.5 ± 4.5	−27.1 ± 0.69	0.249 ± 0.04
B. mori	256 ± 7.2	−18.5 ± 2.5	0.467 ± 0.06

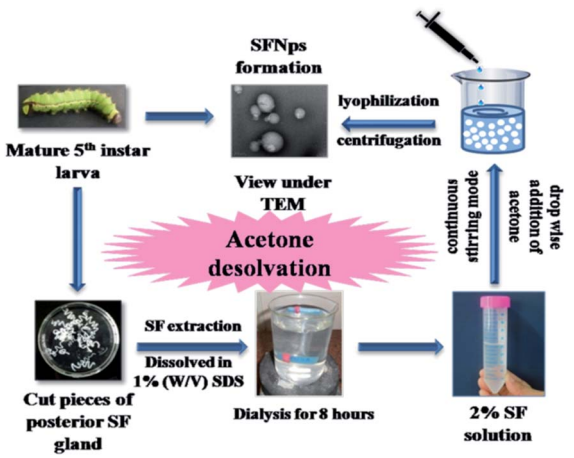

Fig. 1 Scheme representing fabrication of AA-SFNps from matured 5th instar larvae using acetone desolvation procedure.

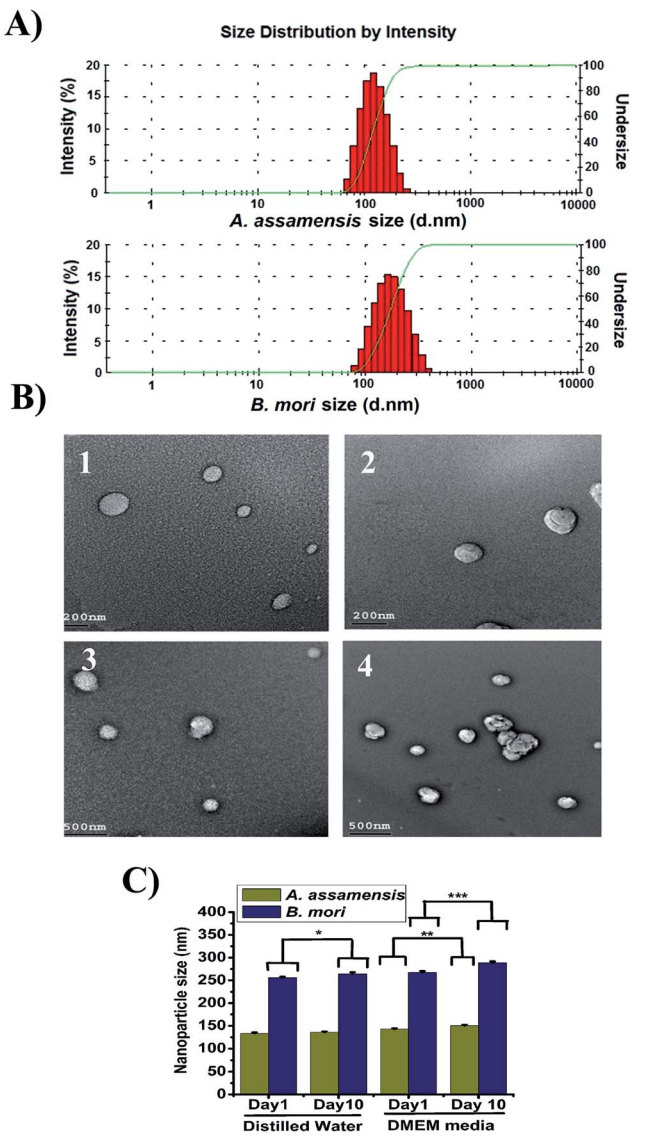

Fig. 2 (A) Size distribution intensity of AA-SFNps and BM-SFNps as revealed by DLS measurements (B) TEM images showing ultra-structure of fabricated AA-SFNps (80–300 nm in diameter) [1,3] with smooth surface and BM-SFNps (120–500 nm) [2, 4] with comparatively rough surface morphology and (C) stability of the nanoparticles at two different time points, $n = 3$, * represents significant statistical difference $p \leq 0.05$.

both AA-SFNps and BM-SFNps. The size range depicted by other non-mulberry SFNps in previous reports have shown similar ranges.[20–22]

The stability of the nanoparticles was measured in distilled water and DMEM media with 10% FBS at two different time intervals (day 1 and day 10) (Fig. 2C). The particles in distilled water of AA-SF did not show any statistical difference in both the day points in comparison with BM-SFNps which showed little increase in size ($p < 0.05$). Both AA-SFNps and BM-SFNps showed a gradual increase in size in cell culture media but the statistical difference was found to be much higher in case of BM-SFNps ($p < 0.001$) in comparison to AA-SFNps ($p < 0.01$). This increase in size is possibly because of adherence of the serum protein onto the surface of the nanoparticles.[11] Overall, AA-SFNps showed greater stability compared to BM-SFNps. Nanoparticles from *B. mori*, *A. mylitta* and *A. pernyi* in earlier reports exhibited potential stability in different biological media which have promoted their utility in different delivery systems.[20–22] Better stability of AA-SFNps in biological media represents potentiality of the nanoparticles to be used as bionanomaterials.

Structural and thermal characterization

Structural conformation of the fabricated nanoparticles was evaluated using FTIR spectroscopy. In AA-SFNps, amide I vibration (C=O stretching) band was represented at 1623 cm^{-1} and amide II (secondary N–H bending), III (C–N and N–H functionalities) bands were represented at 1520 cm^{-1} and 1232 cm^{-1} respectively (Fig. 3A). AA-SF has been reported to be exhibit characteristics bands at 1620 cm^{-1}, 1518 cm^{-1} and 1234 cm^{-1} for amide I, II and III respectively.[26] Since region from 1700–1600 cm^{-1} are representative of amide I and regions from 1540–1520 cm^{-1} and 1300–1220 cm^{-1} are significant for amide II and III respectively, AA-SFNps reveal the persistence of its structural properties even after fabrication which is crucial for maintaining biological properties by the particles in any form.[25,39] BM-SFNps showed characteristics bands at 1620 cm^{-1}, 1515 cm^{-1} and 1228 cm^{-1} for amide I, amide II and an amide III band respectively which also retains required structural characteristics as justified from previous reports.[28,40]

The crystalline structure of the nanoparticles was further analyzed using XRD. Two major peaks were observed for AA-SFNps at 16.7 and 20.2 respectively which represent β-sheet crystalline structure (silk II) and formation of β-sheet secondary conformation and one minor peak at 23.78 that shows a transition from amorphous to crystalline nature (Fig. 3B).[28,40] Overall, these structural features provide more stability to the protein nanoparticles. BM-SFNps showed one broad peak at 20.3 that signifies for β-sheet crystalline structure and one minor peak at 24.08. The results are in agreement with earlier reports on *A. mylitta*, *A. pernyi*, *A. assamensis* and *B. mori* SF in other pure and fabricated forms.[20–22,39]

Thermal properties of SFNps were evaluated using DSC and TGA analysis. DSC results of AA-SFNps displayed first endothermic peak at 116.48 °C and a final degradation peak at about 362.15 °C (Fig. 3C). The data supports recent work carried out on *A. assamensis* SF microparticles as well as earlier reports on *A. assamensis* SF.[24,28] These peaks are representative for loss of moisture and decomposition of the protein molecules. BM-SFNps showed first endothermic peak for moisture loss at 129.54 °C whereas final decomposition peak for *B. mori* was found to be at a lower temperature than AA-SFNps *i.e.* 296.75 °C which shows similar comparative pattern as revealed with *A. assamensis* microparticles.[28] Results exhibited higher thermal stability of the AA-SFNps than BM-SFNps representing greater chemical stability of the non-mulberry AA-SFNps.

TGA results of the fabricated SFNps showed a similar trend. The first percentage weight loss for AA-SFNps was found to be at around 267.6 °C that signifies for disruption of the side chain and second final weight loss resulting in degradation of the protein molecule was observed at 385.4 °C (Fig. 3D). BM-SFNps showed initial breakdown at 246.3 °C and a final degradation at around 334.1 °C. Results clearly reveal greater stability of the AA-SFNps. Data highly supports previous reports on AA-SF and BM-SF.[25,26,28]

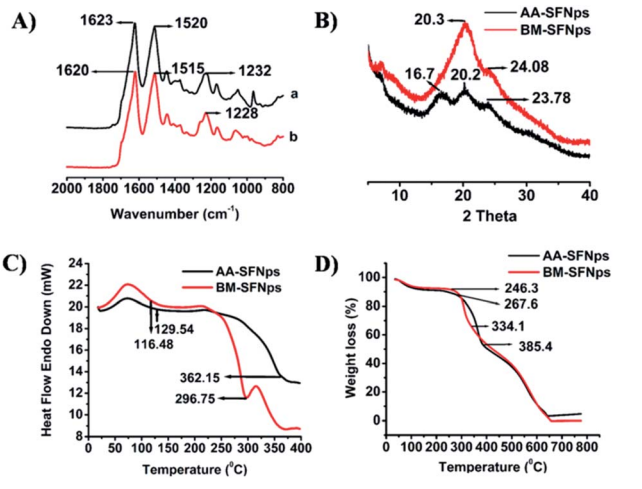

Fig. 3 (A) FTIR analysis of (a) AA-SFNps and (b) BM-SFNps showing amide I, amide II and amide III bonds (B) XRD data showing silk I and silk II structure. (C) DSC and (D) TGA curves of AA-SFNps and BM-SFNps representing degradation peak and percentage weight loss respectively.

Biocompatibility of the SFNps

The biocompatibility of the SFNps was studied using MTT assay. To act as a potent nanocarrier, it is very important to

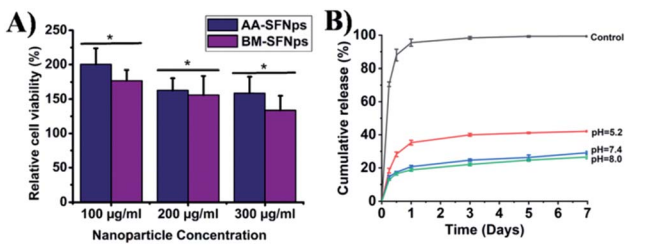

Fig. 4 (A) Cytotoxicity profile of the AA-SFNps and BM-SFNps. $n = 3$, * represents significant statistical difference at $p < 0.05$ (B) drug release profile of DOX from AA-SFNps-DOX under different pH conditions (pH 5.2, 7.4 and 8.0 respectively) at 37 °C for a period of 7 days.

analyse the cytotoxicity profile so that nanoparticles are compatible with the *in vivo* environment. Various factors like size, surface zeta potential, morphology of the nanoparticles *etc.* play a crucial role in cellular uptake and proper interaction with the cell surface.[19] Viability of L-929 cells was studied with different concentrations of AA-SFNps and BM-SFNps (100, 200, and 300 μg ml^{-1}). The results showed significantly higher cell viability in all the concentrations of AA-SFNps ($p > 0.01$) in comparison to BM-SFNps after 24 h of incubation (Fig. 4A). Cells were viable at higher concentrations (*i.e.* 300 μg ml^{-1}) indicating the non-cytotoxic nature of the SFNps. At 100 μg ml^{-1} concentration, cells displayed viability more than TCP (cells grown without any sample, control).[28] This enhanced cell proliferation in AA-SFNps might be due to the presence of cell binding motifs-RGD in the non-mulberry SF protein which provides a better environment for cell attachment and proliferation.[24] The data are in agreement with previous results on a recent study.[25,28] Overall, AA-SFNps satisfy basic criteria to be used as an effective candidate for tissue engineering. In order to study its applicability in drug delivery, AA-SFNps were further evaluated for its drug loading, release study and toxicity profile with anticancer model drug doxorubicin.

Drug loading and encapsulation efficiency

Drug loading of pharmaceutical agents in particles is a key parameter to evaluate the therapeutic efficacy of carriers.[17] Positively charged DOX binds with negatively charged protein nanoparticles through electrostatic interaction.[41] AA-SFNps showed best loading concentration of DOX in the proportion 1 : 1/8. AA-SFNps showed an encapsulation efficiency of 94.47% with 11.81% loading of the model drug. Drug loading was confirmed using FTIR and DLS study. The size of the AA-SFNps-DOX as revealed by DLS was found to be increasing from 190 ± 6.1 nm to 248.03 ± 7.54 nm (Table S1†). The overall surface zeta potential has displayed decreasing value from −28.1 ± 3.4 mV to −17.8 ± 2.83 indicating loading of the positively charged DOX onto its surface thereby reducing the surface zeta potential. This is due to the amino groups of DOX neutralizing the carboxyl group of SF. FTIR results of AA-SFNps-DOX revealed the formation of a new band at 1368 cm^{-1} and shifting of amide II band from 1516 cm^{-1} to 1522 cm^{-1} (Fig. S1†). Variation in structural peaks in AA-SFNps-DOX is clearly visible in comparison to pure DOX and AA-SFNps spectra indicating an interaction between the functional groups.[29]

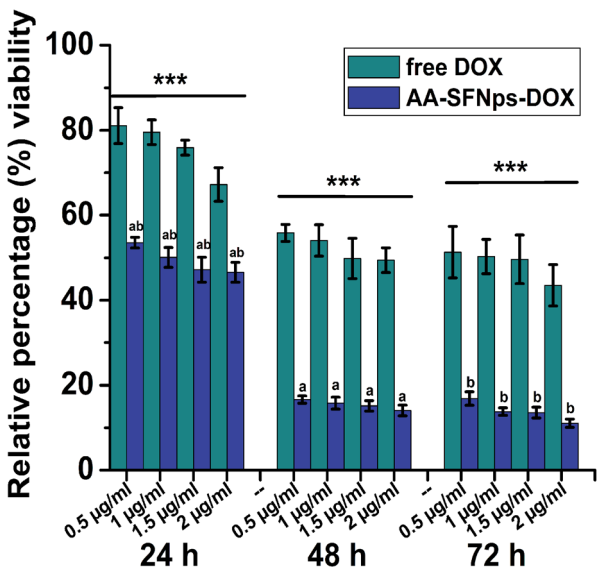

Fig. 5 Cytotoxicity in MDA-MB-231 cell line in terms of relative percentage viability exhibited by free DOX and AA-SFNps-DOX with different concentrations and at different time points, ($n = 4$). Here, *** represents for each concentration, within a single time point both free DOX and AA-SFNps-DOX are highly significant ($p \leq 0.001$), (a and b) represent at same concentration between 24 hour *vs.* 48 hour and 24 hour *vs.* 72 hour respectively, values are highly significant ($p \leq 0.001$) indicating sustained release of the drug.

In vitro release of DOX-loaded AA-SFNps

DOX was loaded electro-statically with AA-SFNps through a charge to charge interaction. DOX being positively charged molecule interacts with negatively charged SFNps through ionic bond forming AA-SFNps-DOX complex. Release of DOX from AA-SFNps-DOX complex showed pH dependence. Cumulative release of DOX at pH 5.2 showed highest percentage release of 42.1 ± 0.4% at day 7 whereas it was found to be 29.16 ± 0.81% and 26.58 ± 1.07% for pH 7.4 and 8.0 respectively (Fig. 4B). Cancer cells grow more favourably under acidic conditions, thus release of anticancer drugs under acidic conditions from nanocarrier encourages and reveals its effectiveness with the drug delivery system.[42] Moreover, AA-SFNps displayed a sustained release profile of DOX with time. Free DOX (control) showed initial burst release of about 70.57 ± 1.4% at 6 hours whereas only 18.34 ± 1.4% of DOX from AA-SFNps-DOX complex was released at the same period of time at pH 5.2. AA-SFNps particles showed a more sustained release of DOX after day 3 and at day 5 (∼2%) and 7 (∼1%) respectively. Results clearly reveal controlled release of the drug and their possibilities in reducing dose-dependent toxicity through sustain release and thereby enhancing the delivery of the drug in the target site.[2,3] Overall, fabricated AA-SFNps show its potentiality to be used as a suitable candidate for future drug delivery systems.

Cytotoxicity of AA-SFNps-DOX

In vitro cytotoxicity profile of the drug loaded nanoparticles revealed higher cytotoxicity towards MDA-MB-231 cell line in comparison to the free drug (DOX) in all the time points (Fig. 5). This highly significant difference in relative percentage viability ($p \leq 0.001$) was probably because of the rapid internalization of the

Table 3 IC_{50} (μg ml^{-1}) calculated from the cytotoxicity study of free DOX and AA-SFNps-DOX

Time (in hours)	24 h	48 h	72 h
Free DOX	3.225 ± 0.60	1.577 ± 0.22	1.422 ± 0.47
AA-SFNps-DOX	1.422 ± 0.14	0.487 ± 0.03	0.472 ± 0.03

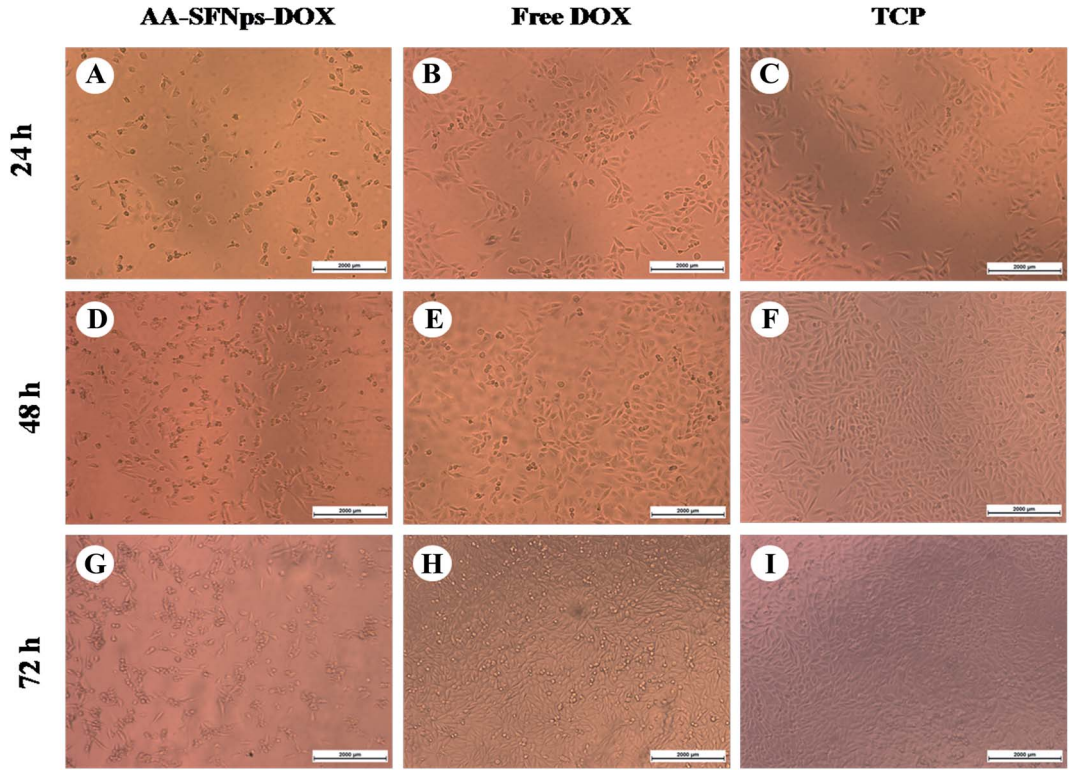

Fig. 6 Representative microscopic images showing cell morphology of MDA-MB-231 cells after AA-SFNps-DOX (A, D and G) and free DOX treatment (B, E and H) at 24 h, 48 h and 72 hours respectively. Cells grown without any sample was taken as control (TCP), (C, F and I). A drug concentration of 1 μg ml^{-1} for both free DOX and DOX loaded nanoparticles were used for treatment in each time points for the present study.

nanocarrier mediated DOX particles (AA-SFNps-DOX) by the cancer cells.[43] With increase in incubation time of AA-SFNps-DOX particles from 24 h to 48 h, there was a rapid decrease in percentage of viable MDA-MB-231 cells from ~53% to ~16% at 0.5 μg ml^{-1} of the drug-loaded nanoparticles. A similar relative trend was observed for all the concentrations with increasing incubation time from 24 h to 48 h and likewise with 24 h and 72 h of the AA-SFNPs-DOX indicating sustained release of the drug with time. Such observed behaviour might encourage the role of the nanocarrier in reducing the problems associated with dose-dependent toxicity of the DOX molecule and thereby favouring in delivery of the drug to the proper target site.[1–4] IC_{50} values of AA-SFNps-DOX at each time point was found to be approximately three times lesser than the free DOX molecule indicating potentiality of the drug to be used as nanocarrier in drug delivery systems (Table 3).

Cell morphology study

The efficacy of the drug-loaded nanoparticles was evaluated by observing the morphological changes in MDA-MB-231 cells after treatment with a fixed concentration (1 μg ml^{-1}) of DOX for both free DOX and AA-SFNPs-DOX at three different time points (*i.e.* 24 h, 48 h and 72 hours). At 24 h, the morphology of the normal cells in control wells (TCP) was found to be spindle in shape with proper spreading, whereas the wells with free DOX showed fewer dead cells along with normally spread cells when compared to TCP (Fig. 6). This percentage was found to be even much higher when wells containing AA-SFNps-DOX were observed. The number of dead cells was around 40% in AA-SFNPs-DOX at 24 hours. With increase in time points (at 48 h and 72 h), the sensitivity of the AA-SFNPs-DOX towards MDA-MB-231 cell line was found to be prominently higher leading to more cell death in comparison to the free DOX. This increase in cytotoxicity with the same concentration of the drug in AA-SFNPs-DOX might be attributed to the rapid internalization by the cells resulting in proper delivery of the drug to the target site and hence cell death.[2,3]

Conclusions

The need for exploration of SF from different species in order to fabricate potential materials with enhanced properties has always been of utmost demand in the recent era of biomedical engineering.[6,7] This is the first report of preparing AA-SFNps using simple desolvation method and evaluation of potentiality to be used in the field of tissue engineering and drug delivery. Non-mulberry SF is known for presence of RGD sequence favorable for cell attachment and proliferation which is a key requirement to be used as biomaterials.[23] Smooth, stable nanoparticles with a size range varying from 80–300 nm in diameter were formed which showed sustained release of model drug DOX with highest % release at acidic pH 5.2. Moreover, DOX loaded *A. assamensis* nanoparticles are found to be more effective to killing MDA-MB-231 cells in comparison to the free drug indicating its contribution towards target centric

drug delivery. Overall, this study will provide an insight to the potentiality of the *A. assamensis* SF nanoparticles to be used for future drug delivery and tissue engineering applications.

Conflicts of interest

There are no conflicts to declare.

Acknowledgements

The authors would like to acknowledge the Department of Biotechnology (BT/264/NE/TBP/2011 dtd.11/04/2012), Govt. of India for providing the financial support, the host institute, Institute of Advanced Study in Science and Technology (IASST), Assam, India for providing the central instrumentation facility and SAIF, NEHU for performing TEM analysis. The authors also like to thank Dr Devasish Chowdhury, Associate Professor II, Physical Sciences Division, IASST for his kind suggestions during final corrections in the manuscript and Miss Bhaswati Kashyap, Drug Discovery Laboratory, IASST for providing cells and her support during the cell culture experiments.

References

1 Z. Zhao, Y. Li and M.-B. Xie, *Int. J. Mol. Sci.*, 2015, **16**, 4880–4903.
2 H. Li, J. Tian, A. Wu, J. Wang, C. Ge and Z. Sun, *Int. J. Nanomed.*, 2016, **11**, 4373.
3 Y. Tian, X. Jiang, X. Chen, Z. Shao and W. Yang, *Adv. Mater.*, 2014, **26**, 7393–7398.
4 S. Yu, W. Yang, S. Chen, M. Chen, Y. Liu, Z. Shao and X. Chen, *RSC Adv.*, 2014, **4**, 18171–18177.
5 D. Naskar, R. Barua, A. Ghosh and S. Kundu, in *Silk Biomaterials for Tissue Engineering and Regenerative Medicine*, Elsevier, 2014, ch. 1, pp. 3–40.
6 G. H. Altman, F. Diaz, C. Jakuba, T. Calabro, R. L. Horan, J. Chen, H. Lu, J. Richmond and D. L. Kaplan, *Biomaterials*, 2003, **24**, 401–416.
7 K. Numata and D. L. Kaplan, *Adv. Drug Delivery Rev.*, 2010, **62**, 1497–1508.
8 E. Wenk, H. P. Merkle and L. Meinel, *J. Controlled Release*, 2011, **150**, 128–141.
9 S. E. Wharram, X. Zhang, D. L. Kaplan and S. P. McCarthy, *Macromol. Biosci.*, 2010, **10**, 246–257.
10 A. Schneider, X. Wang, D. Kaplan, J. Garlick and C. Egles, *Acta Biomater.*, 2009, **5**, 2570–2578.
11 S. Wang, T. Xu, Y. Yang and Z. Shao, *ACS Appl. Mater. Interfaces*, 2015, **7**, 21254–21262.
12 V. Gupta, A. Aseh, C. N. Ríos, B. B. Aggarwal and A. B. Mathur, *Int. J. Nanomed.*, 2009, **4**, 115.
13 P. Wu, Q. Liu, R. Li, J. Wang, X. Zhen, G. Yue, H. Wang, F. Cui, F. Wu and M. Yang, *ACS Appl. Mater. Interfaces*, 2013, **5**, 12638–12645.
14 B. Subia and S. Kundu, *Nanotechnology*, 2012, **24**, 035103.
15 L. Xiao, G. Lu, Q. Lu and D. L. Kaplan, *ACS Biomater. Sci. Eng.*, 2016, **2**, 2050–2057.
16 A. A. Lozano-Pérez, A. L. Gil, S. A. Pérez, N. Cutillas, H. Meyer, M. Pedreño, S. D. Aznar-Cervantes, C. Janiak, J. L. Cenis and J. Ruiz, *Dalton Trans.*, 2015, **44**, 13513–13521.
17 N. Sun, R. Lei, J. Xu, S. C. Kundu, Y. Cai, J. Yao and Q. Ni, *J. Mater. Sci.*, 2019, **54**, 3319–3330.
18 B. Subia, S. Chandra, S. Talukdar and S. C. Kundu, *Integr. Biol.*, 2013, **6**, 203–214.
19 J. Kundu, Y.-I. Chung, Y. H. Kim, G. Tae and S. Kundu, *Int. J. Pharm.*, 2010, **388**, 242–250.
20 J. Wang, S. Zhang, T. Xing, B. Kundu, M. Li, S. C. Kundu and S. Lu, *Int. J. Biol. Macromol.*, 2015, **79**, 316–325.
21 J. Wang, Z. Yin, X. Xue, S. Kundu, X. Mo and S. Lu, *Int. J. Mol. Sci.*, 2016, **17**, 2012.
22 X. Xue, H. Fu and S. Lu, *Nano Research & Applications*, 2017, **3**, 1–8.
23 A. Gupta, K. Mita, K. P. Arunkumar and J. Nagaraju, *Sci. Rep.*, 2015, **5**, 12706.
24 S. Kar, S. Talukdar, S. Pal, S. Nayak, P. Paranjape and S. Kundu, *Tissue Eng. Regener. Med.*, 2013, **10**, 200–210.
25 N. Kasoju, R. R. Bhonde and U. Bora, *Mater. Lett.*, 2009, **63**, 2466–2469.
26 S. Dutta, B. Talukdar, R. Bharali, R. Rajkhowa and D. Devi, *Biopolymers*, 2013, **99**, 326–333.
27 D. Devi, N. S. Sarma, B. Talukdar, P. Chetri, K. Baruah and N. N. Dass, *J. Text. Inst.*, 2011, **102**, 527–533.
28 N. Bhardwaj, R. Rajkhowa, X. Wang and D. Devi, *Int. J. Biol. Macromol.*, 2015, **81**, 31–40.
29 D. Agudelo, P. Bourassa, J. Bruneau, G. Berube, E. Asselin and H.-A. Tajmir-Riahi, *PLoS One*, 2012, **7**, e43814.
30 J. Prados, C. Melguizo, R. Ortiz, C. Velez, P. J. Alvarez, J. L. Arias, M. A. Ruiz, V. Gallardo and A. Aranega, *Anti-Cancer Agents Med. Chem.*, 2012, **12**, 1058–1070.
31 B. B. Mandal and S. Kundu, *Biotechnol. Bioeng.*, 2008, **99**, 1482–1489.
32 H. J. Jin, J. Park, V. Karageorgiou, U. J. Kim, R. Valluzzi, P. Cebe and D. L. Kaplan, *Adv. Funct. Mater.*, 2005, **15**, 1241–1247.
33 D. N. Rockwood, R. C. Preda, T. Yücel, X. Wang, M. L. Lovett and D. L. Kaplan, *Nat. Protoc.*, 2011, **6**, 1612.
34 K. Langer, S. Balthasar, V. Vogel, N. Dinauer, H. Von Briesen and D. Schubert, *Int. J. Pharm.*, 2003, **257**, 169–180.
35 C. Weber, C. Coester, J. Kreuter and K. Langer, *Int. J. Pharm.*, 2000, **194**, 91–102.
36 D. Verma, N. Gulati, S. Kaul, S. Mukherjee and U. Nagaich, *J. Pharm.*, 2018, **2018**, 1–17.
37 A. Jain, S. K. Singh, S. K. Arya, S. C. Kundu and S. Kapoor, *ACS Biomater. Sci. Eng.*, 2018, **4**, 3939–3961.
38 E. Fröhlich, *Int. J. Nanomed.*, 2012, **7**, 55–77.
39 J. Kong and S. Yu, *Acta Biochim. Biophys. Sin.*, 2007, **39**, 549–559.
40 X. Hu, D. Kaplan and P. Cebe, *Macromolecules*, 2006, **39**, 6161–6170.
41 D. H. Jo, J. H. Kim, T. G. Lee and J. Hun Kim, *Nanomedicine*, 2015, **11**, 1603–1601.
42 E. S. Lee, K. Na and Y. H. Bae, *J. Controlled Release*, 2003, **91**, 103–113.
43 R. Lupertz, W. Watjen, R. Kahl and Y. Chovolou, *Toxicology*, 2010, **271**, 115–121.

